

Cubic Double Perovskites Host Noncoplanar Spin Textures

Joseph A. M. Paddison,^{1,*} Hao Zhang,² Jiaqiang Yan,¹ Matthew J. Cliffe,³ Seung-Hwan Do,¹ Shang Gao,^{1,4} Matthew B. Stone,⁴ David Dahlbom,² Kipton Barros,⁵ Cristian D. Batista,⁶ and Andrew D. Christianson^{1,†}

¹*Materials Science and Technology Division, Oak Ridge National Laboratory, Oak Ridge, TN 37831, USA*

²*Department of Physics and Astronomy, University of Tennessee, Knoxville, Tennessee 37996, USA*

³*School of Chemistry, University of Nottingham, Nottingham NG7 2RD, UK*

⁴*Neutron Scattering Division, Oak Ridge National Laboratory, Oak Ridge, Tennessee 37831, USA*

⁵*Theoretical Division, Los Alamos National Laboratory, Los Alamos, New Mexico 87545, USA*

⁶*Department of Physics and Astronomy, The University of Tennessee, Knoxville, Tennessee 37996, USA*

Magnetic materials with noncoplanar magnetic structures can show unusual physical properties driven by nontrivial topology. Topologically-active states are often multi- \mathbf{q} structures, which are challenging to stabilize in models and to identify in materials. Here, we use inelastic neutron-scattering experiments to show that the insulating double perovskites Ba_2YRuO_6 and $\text{Ba}_2\text{LuRuO}_6$ host a noncoplanar 3- \mathbf{q} structure on the face-centered cubic lattice. Quantitative analysis of our neutron-scattering data reveals that these 3- \mathbf{q} states are stabilized by biquadratic interactions. Our study identifies double perovskites as a highly promising class of materials to realize topological magnetism, elucidates the stabilization mechanism of the 3- \mathbf{q} state in these materials, and establishes neutron spectroscopy on powder samples as a valuable technique to distinguish multi- \mathbf{q} from single- \mathbf{q} states, facilitating the discovery of topologically-nontrivial magnetic materials.

Most magnetic materials order with simple magnetic structures in which spins are collinear or coplanar. Noncoplanar magnetic structures are relatively rare, but are of great current interest, because they can exhibit topological character and exotic physical properties [1, 2]. For example, the finite scalar spin chirality of noncoplanar spin textures can generate a topological magneto-optical effect [3] and anomalous quantum Hall effect [4, 5], even in the absence of spin-orbit coupling. Topologically-nontrivial spin textures are typically multi- \mathbf{q} structures, which superpose magnetic modulations with symmetry-related wavevectors \mathbf{q} [2]. Multi- \mathbf{q} spin textures with long-wavelength modulations, such as skyrmion and hedgehog crystals, are well-studied as hosts of topology-driven phenomena [6–8]. In this context, multi- \mathbf{q} antiferromagnets are increasingly important [9], because they offer higher densities of topological objects with the potential to generate stronger physical responses [10].

To probe the relationships between spin structure, interactions, topology, and physical response, it is crucial to identify real materials that host noncoplanar spin textures. This has proved a challenging task, for three main reasons. First, it is necessary to identify noncoplanar spin textures that are robust to subleading effects such as magnetic anisotropies, spin-lattice coupling [11, 12], fluctuations [13–16], and anisotropic interactions [17], which usually favor collinear states. Second, most noncoplanar states are found in metals, such as USb [18, 19] and γ - Mn alloys [20–25], and are often stable only under an applied magnetic field [6, 26]. On the one hand, itinerant electrons can support the generation of physical responses; on the other hand, modeling the magnetic interactions of metals presents fundamental challenges [27–32], such that insulators are often more suitable as model materials. Third, powder neutron-diffraction measurements play a central role in solving magnetic structures, but suffer from a “multi- \mathbf{q} problem”: Such measurements are generally unable to distinguish 1- \mathbf{q} from multi- \mathbf{q} structures [33]. Therefore,

multi- \mathbf{q} spin textures are challenging to stabilize in models, and to identify in real materials.

Here, we identify the Mott-insulating double perovskites Ba_2YRuO_6 and $\text{Ba}_2\text{LuRuO}_6$ [34–37] as prototypical examples of noncoplanar 3- \mathbf{q} magnetism on the face-centered cubic (FCC) lattice in zero magnetic field. We obtain evidence for 3- \mathbf{q} magnetism from a spin-wave analysis of neutron spectroscopy data. By optimizing the magnetic structure and interactions simultaneously against our data, we show that the 3- \mathbf{q} structure is stabilized by biquadratic interactions within an antiferromagnetic Heisenberg-Kitaev model. Our study experimentally establishes that noncoplanar multi- \mathbf{q} states are stabilized in frustrated FCC antiferromagnets, identifies cubic double perovskites as model materials to realize this behavior, and identifies guiding principles to facilitate design of materials with noncoplanar states.

Our study is motivated by theoretical results for the FCC antiferromagnet [13, 38–40]. The nearest-neighbor Heisenberg-Kitaev spin Hamiltonian on the FCC lattice can be written as

$$H = J \sum_{\langle i,j \rangle} \mathbf{S}_i \cdot \mathbf{S}_j + K \sum_{\langle i,j \rangle_\gamma} S_i^\gamma S_j^\gamma, \quad (1)$$

where \mathbf{S}_i is a Ru^{5+} spin with quantum number $S = 3/2$, J and K denote the Heisenberg and Kitaev interactions, respectively, and $\gamma \in \{x, y, z\}$ is perpendicular to the cubic plane containing the bond between neighbors $\langle i, j \rangle$. For antiferromagnetic $J > 0$ only, the model is frustrated, and orderings with $\mathbf{q} \in [1, q, 0]$ are degenerate [13, 39, 40]. The degenerate manifold includes $\mathbf{q} = [1, 0, 0]$ (“Type I”) ordering, which is favored by fluctuations [13, 14, 41] and is observed in Ba_2YRuO_6 and $\text{Ba}_2\text{LuRuO}_6$ [34]. Henceforth, we therefore restrict our discussion to $\mathbf{q} = [1, 0, 0]$ ordering. For a collinear structure, spins may be either parallel or perpendicular to \mathbf{q} ; the former is favored by $K < 0$ and the latter by $K > 0$ [38–40].

Figure 1(a) shows the collinear (1- \mathbf{q}) and noncollinear

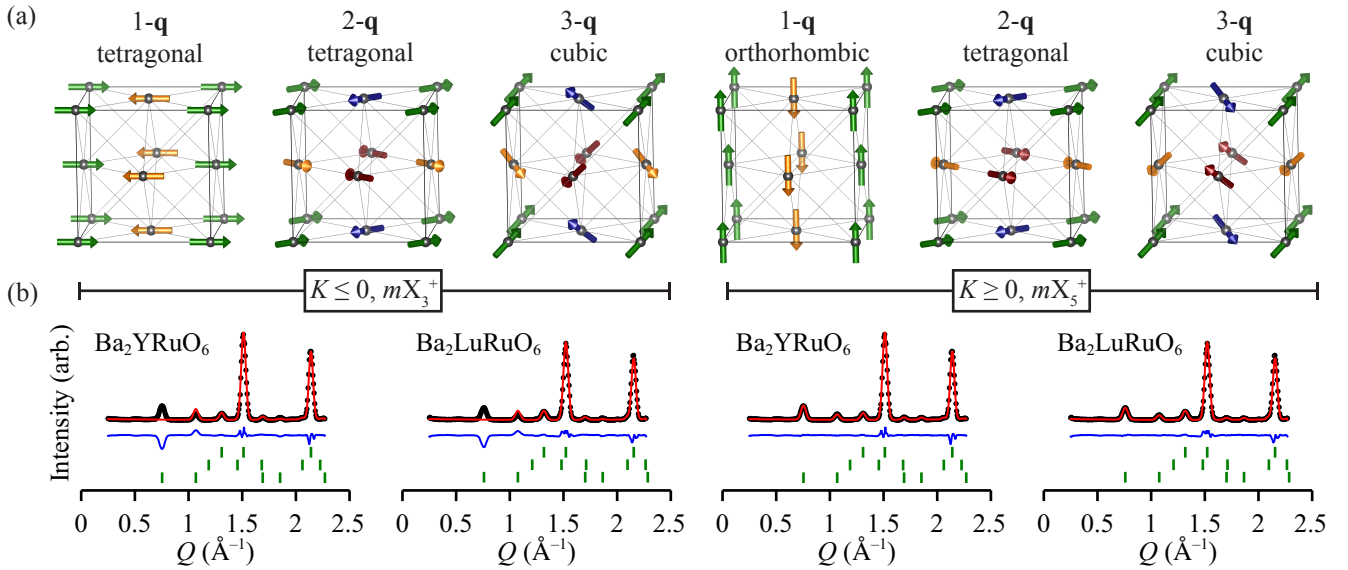


Figure 1. (a) Symmetry-allowed magnetic structures with propagation vector $\mathbf{q} = [1, 0, 0]$ on the FCC lattice for Ba_2MRuO_6 (space group $Fm\bar{3}m$; $a = 8.29$ and 8.24 \AA for $M = \text{Y}$ and Lu , respectively). The 1- \mathbf{q} , 2- \mathbf{q} , and 3- \mathbf{q} structures are shown for the mX_3^+ irrep (left) and the mX_5^+ irrep (right). Spins along different directions are colored differently; note that 1- \mathbf{q} , 2- \mathbf{q} , and 3- \mathbf{q} structures have $\langle 100 \rangle$, $\langle 110 \rangle$, and $\langle 111 \rangle$ spin directions, respectively. (b) Elastic scattering data ($-1.3 \leq E \leq 1.3$ meV) measured at $T = 5$ K with $E_i = 11.8$ meV for Ba_2YRuO_6 and $\text{Ba}_2\text{LuRuO}_6$ (black circles), Rietveld refinements (red lines), and data – fit (blue lines). Tick marks show (top to bottom): nuclear, impurity M_2O_3 , and magnetic phases. The mX_3^+ irrep (left) does not reproduce our data, whereas the mX_5^+ irrep (right) agrees well with our data.

(multi- \mathbf{q}) structures associated with Type I antiferromagnetism. A remarkable property of the FCC lattice is that 1- \mathbf{q} , 2- \mathbf{q} , and 3- \mathbf{q} structures are energetically degenerate for *all* bilinear interactions for which Type I ordering is stable [39, 40]. Moreover, uniaxial anisotropy ($\sim S_z^2$) and antisymmetric exchange terms are forbidden by $Fm\bar{3}m$ symmetries, and quartic anisotropy ($\sim S_x^4 + S_y^4 + S_z^4$) is forbidden for $S = 3/2$ operators in a cubic environment. Consequently, interactions that would usually favor collinear magnetic structures are inactive in the $S = 3/2$ FCC antiferromagnet. This remarkable property potentially allows noncollinear structures to appear.

To identify candidate systems for 3- \mathbf{q} spin textures among the diverse magnetic ground states of double perovskites [42–50], we consider two criteria: Type I antiferromagnetic ordering, and strictly cubic symmetry below the magnetic ordering temperature, T_N . The second criterion is key because 3- \mathbf{q} structures have cubic symmetry, while 1- \mathbf{q} and 2- \mathbf{q} structures have tetragonal or orthorhombic symmetry that could drive a crystallographic distortion *via* spin-lattice coupling [Figure 1(a)]. We investigate Ba_2YRuO_6 and $\text{Ba}_2\text{LuRuO}_6$ because they are chemically well-ordered and show no evidence for low-temperature deviations from cubic symmetry [34, 36]. Moreover, recent first-principles calculations predict that their magnetic structures might not be collinear [51], in apparent contradiction with interpretations of previous experiments [34].

We prepared ~ 8 g polycrystalline samples of Ba_2YRuO_6 and $\text{Ba}_2\text{LuRuO}_6$ by solid-state reaction [52]. Rietveld refinement revealed stoichiometric samples with minor Lu_2O_3

(1.94 wt.%) or Y_2O_3 (0.65 wt.%) impurities. The magnetic ordering temperature $T_N \approx 37$ K is the same for both samples, and is suppressed compared to the Weiss temperature $\theta \sim -500$ K, indicating strong magnetic frustration [36]. We performed inelastic neutron-scattering measurements on the SEQUOIA instrument at ORNL [53] using incident neutron energies $E_i = 62$ and 11.8 meV, yielding elastic energy resolutions $\delta_{\text{ins}} \approx 1.68$ and 0.27 meV, respectively.

Figure 1(b) shows magnetic Rietveld refinements to our elastic neutron-scattering data, measured with $E_i = 11.8$ meV at $T \approx 5$ K. Applying the $\mathbf{q} = [1, 0, 0]$ propagation vector to $Fm\bar{3}m$ crystal symmetry generates two magnetic irreducible representations (irreps), notated mX_3^+ and mX_5^+ [54, 55]. These irreps can be distinguished by their magnetic Bragg profiles. The mX_5^+ irrep agrees well with our elastic-scattering data for both materials; we obtain ordered magnetic moment lengths of $2.56(2)$ and $2.43(2) \mu_B$ per Ru for Ba_2YRuO_6 and $\text{Ba}_2\text{LuRuO}_6$, respectively, from Rietveld refinement. Since the magnetic form factor for Ru^{5+} is not known, we tested several $4d$ magnetic form factors [56]; while this choice does not qualitatively affect our results, the form factor for Zr^{4+} (isoelectronic with Ru^{5+}) yields optimal agreement with our data and is used throughout. In contrast to the mX_5^+ irrep, the mX_3^+ irrep strongly disagrees with our data, as it yields zero intensity for the strong (100) magnetic Bragg peak. This can be understood intuitively for a collinear 1- \mathbf{q} structure, because neutrons are only sensitive to spin components perpendicular to the scattering wavevector, and the mX_3^+ irrep has $\mathbf{S} \parallel \mathbf{q}$ while the mX_5^+ irrep has $\mathbf{S} \perp \mathbf{q}$ [Figure 1(a)]. A previous elas-

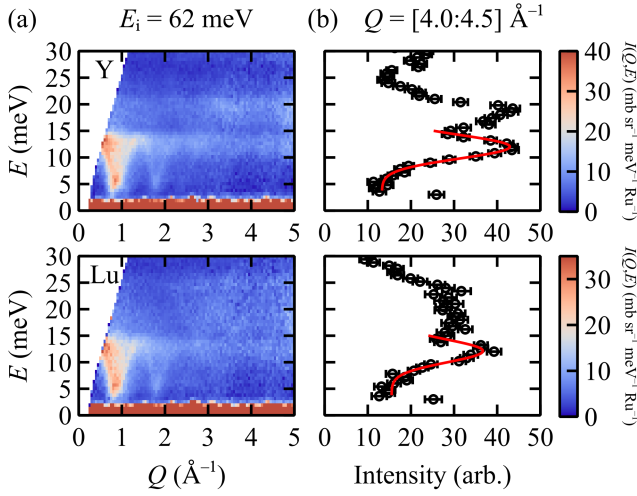


Figure 2. Broadband inelastic neutron-scattering data ($E_i = 62$ meV) measured at $T = 5$ K for Ba_2YRuO_6 (upper panels) and $\text{Ba}_2\text{LuRuO}_6$ (lower panels), showing (a) intensity as a color plot, and (b) energy dependence integrated over $4.0 \leq Q \leq 4.5 \text{ \AA}^{-1}$, where experimental data are shown as black circles, and Gaussian fits to the ~ 14 meV phonon band as red lines.

tic neutron-scattering study of Ba_2YRuO_6 and $\text{Ba}_2\text{LuRuO}_6$ considered only collinear 1-q structures [34], but could not rule out multi- \mathbf{q} structures, due to the multi- \mathbf{q} problem.

To overcome the multi- \mathbf{q} problem, we consider the energy dependence of our neutron-scattering data [57]. Figure 2(a) shows our inelastic data measured with $E_i = 62$ meV at $T \approx 5$ K. A structured inelastic signal appears at $T < T_N$ for small scattering wavevectors, $Q \lesssim 2 \text{ \AA}^{-1}$, which we identify as magnon scattering. The top of the magnetic band overlaps with an intense phonon signal for $Q \gtrsim 2 \text{ \AA}^{-1}$. Figure 2(b) shows the scattering intensity integrated over $4.0 \leq Q \leq 4.5 \text{ \AA}^{-1}$, from which we extract the average energy E_{ph} and width σ_{ph} of this phonon band *via* Gaussian fits for each material. The energy overlap of magnon and phonon modes suggests that spin-lattice coupling may be significant, which we consider further below.

Our starting point for modeling the magnetic scattering is the Heisenberg-Kitaev model, Eq. (1). For all models, we require $J > 0$ and $K > 0$ to stabilize mX_5^+ ordering. We consider three additional interactions in turn. First, the symmetric off-diagonal interaction $H_\Gamma = \Gamma \sum_{\langle i,j \rangle_\gamma} (S_i^\alpha S_j^\beta + S_i^\beta S_j^\alpha)$ is the only additional bilinear nearest-neighbor interaction allowed by symmetry. Second, the Heisenberg next-nearest neighbor interaction $H_2 = J_2 \sum_{\langle\langle i,j \rangle\rangle} \mathbf{S}_i \cdot \mathbf{S}_j$ has been invoked for Ba_2YRuO_6 [37]; we require $J_2 \leq 0$ to stabilize Type I ordering. Third, the nearest-neighbor biquadratic coupling $H_{\text{bq}} = J_{\text{bq}} \sum_{\langle i,j \rangle} (\mathbf{S}_i \cdot \mathbf{S}_j)^2$ has been invoked in density-functional-theory calculations for $4d$ double perovskites due to their increased electron hopping relative to $3d$ analogs [51]. For $J_{\text{bq}} = 0$, the classical energy of 1-q , 2-q , and 3-q structures is equal for all K , Γ , and J_2 that stabilize Type I ordering. Nonzero J_{bq} removes this degeneracy, and stabilizes

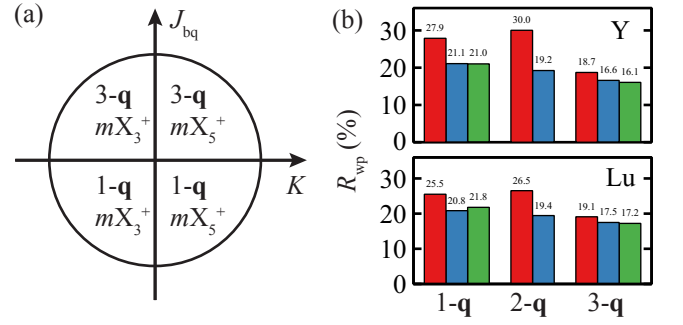


Figure 3. (a) Schematic phase diagram showing the magnetic ground states of the J - K - J_{bq} model. (b) Goodness-of-fit metric R_{wp} for candidate magnetic structures and interaction models of Ba_2YRuO_6 (upper graph) and $\text{Ba}_2\text{LuRuO}_6$ (lower graph). The graphs show R_{wp} for refinements of the Heisenberg-Kitaev (J - K) model including a third refined parameter Γ (red bars), J_2 (blue bars), or J_{bq} (green bars); note that the 2-q structure is stable only for $J_{\text{bq}} = 0$.

	J (K)	K (K)	J_{bq} (K)	A (meV)
Ba_2YRuO_6	21.85(3)	0.39(1)	1.32(2)	0.97(3)
$\text{Ba}_2\text{LuRuO}_6$	22.27(4)	0.36(2)	1.17(3)	2.25(5)

Table I. Refined values of magnetic interaction parameters for the J - K - J_{bq} model and 3-q structure. Uncertainties indicate 1σ statistical confidence intervals.

1-q ordering for $J_{\text{bq}} < 0$ and 3-q ordering for $J_{\text{bq}} > 0$ [Figure 3(a)]. Importantly, since single-ion anisotropies are forbidden for $S = 3/2$ in a cubic environment, biquadratic exchange is the only physically-plausible mechanism that can remove the degeneracy of 1-q and 3-q structures.

We performed extensive fits to our inelastic neutron-scattering data to optimize the magnetic structure and interactions simultaneously. For each structure associated with the mX_5^+ irrep (1-q , 2-q , or 3-q), we optimized three spin Hamiltonian parameters (J , K , and either Γ , J_2 , or J_{bq}) against the broadband inelastic data shown in Figure 4(a) and the energy dependence near the (100) magnetic Bragg position shown in Figure 4(b). The powder-averaged magnon spectrum was calculated within a renormalized linear spin-wave theory [58] using the SpinW program [59]. The renormalization factor, which takes into account higher-order corrections in the $1/S$ expansion, is strictly necessary to extract a correct value of J_{bq} , since the unrenormalized spin-wave theory would lead to a value of J_{bq} that is 2.25 times smaller than the correct value [60]. The parameter values were optimized to minimize the sum of squared residuals using nonlinear least-squares refinement [52]. We calculated the energy-dependent broadening of the magnon spectrum as $\delta(E) = \delta_{\text{ins}}(E) + Ae^{-(E-E_{\text{ph}})^2/2\delta_{\text{ph}}^2}$, where $\delta(E)$ is the overall Gaussian energy width, $\delta_{\text{ins}}(E)$ is the instrumental resolution, and A is a refined parameter that phenomenologically accounts for magnon broadening due to coupling with phonons at $E \sim E_{\text{ph}}$.

Figure 4(a) compares our broadband inelastic data ($E_i = 62$ meV) with the best fit for each of the 1-q , 2-q , and 3-q

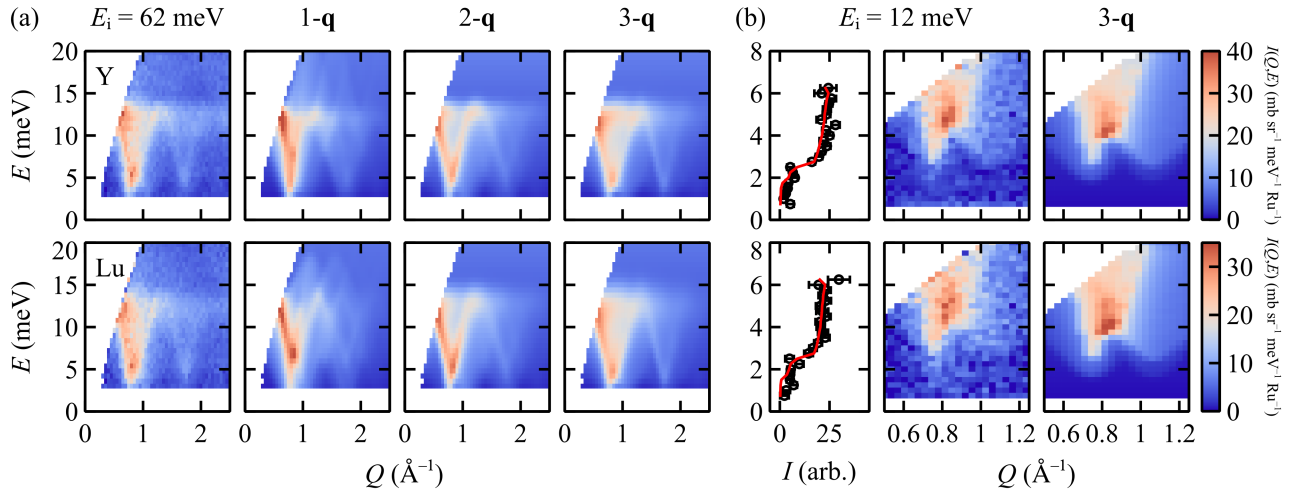


Figure 4. (a) Broadband inelastic neutron-scattering data ($E_i = 62$ meV) and optimal spin-wave fits for different magnetic structures, showing (left to right) experimental data, 1- \mathbf{q} fit, 2- \mathbf{q} fit, and 3- \mathbf{q} fit. (b) Low-energy inelastic neutron-scattering data ($E_i = 11.8$ meV) and 3- \mathbf{q} model calculations, showing (left to right) a cut at $Q = 0.7450 \pm 0.0175 \text{ \AA}^{-1}$ comparing experimental data (black circles) and spin-wave fit (red lines), experimental data as a Q - E slice, and spin-wave calculation.

structures. The data show two V-shaped features centered at ≈ 0.85 and $\approx 1.70 \text{ \AA}^{-1}$, with a sharp cutoff of magnetic signal for energies above ~ 14 meV. For both materials, these characteristics are best reproduced by the 3- \mathbf{q} structure, while the 1- \mathbf{q} structure disagrees with our experimental data. These observations are confirmed by the goodness-of-fit metric R_{wp} , shown in Figure 3(b). For both materials and for every interaction model we considered, the 3- \mathbf{q} structure yields better agreement with our data than the 1- \mathbf{q} or 2- \mathbf{q} structures. Notably, the goodness-of-fit is more sensitive to the structure than the precise magnetic interactions; indeed, the main differences between 1- \mathbf{q} and 3- \mathbf{q} spectra are apparent for Heisenberg exchange only [52]. The global best fit is for the 3- \mathbf{q} structure and J , K , and J_{bq} interactions with the refined values given in Table I. The refined values of A indicate significant magnon broadening, which is larger for $\text{Ba}_2\text{LuRuO}_6$ and is likely due to magnon-phonon coupling. Importantly, for both materials, the biquadratic term is significant, with $J_{\text{bq}}/J \sim 0.06$. Hence, our key results are that only the 3- \mathbf{q} spin texture agrees well with our neutron data, and this state is stabilized by biquadratic interactions in Ba_2YRuO_6 and $\text{Ba}_2\text{LuRuO}_6$.

Our model provides insight into the mechanism of gap opening [35]. Figure 4(b) compares our low-energy inelastic data ($E_i = 11.8$ meV) with the 3- \mathbf{q} magnon spectrum for the optimal J - K - J_{bq} model [Table I]. This calculation reproduces the observed ≈ 2.8 meV gap, unlike the J - K - J_2 model that yields the next-best R_{wp} [52]. Since single-ion anisotropies are forbidden here, the mechanism of gap opening is subtle. If $K = 0$, there is no gap, because the energy of the Heisenberg and biquadratic terms is unchanged by global spin rotations. For $K > 0$, whether a gap opens depends on both structure and interactions. If the structure is 1- \mathbf{q} with $J_{\text{bq}} < 0$, the classical energy is unchanged by global spin rotations in the plane perpendicular to \mathbf{q} . In this case, there is no gap at the linear

spin-wave level; a gap is generated only by magnon interactions in the quantum ($S = 1/2$) limit [61]. By contrast, if the structure is 3- \mathbf{q} with $J_{\text{bq}} > 0$, a gap is present at the linear spin-wave level, because $J_{\text{bq}} > 0$ and $K > 0$ together favor $\langle 111 \rangle$ spin alignment. Since Ba_2YRuO_6 and $\text{Ba}_2\text{LuRuO}_6$ are not in the quantum limit, the experimental observation of a gap supports the presence of biquadratic and Kitaev interactions in a 3- \mathbf{q} structure.

We have shown that the magnetic ground states of Ba_2YRuO_6 and $\text{Ba}_2\text{LuRuO}_6$ are noncoplanar 3- \mathbf{q} structures stabilized by biquadratic interactions. Macroscopic topological physical responses may be generated synthesizing thin films of these materials with $[111]$ strain [62]. Our experimental results strikingly confirm recent first-principles predictions [51]. The positive sign of J_{bq} suggests that the effect of inter-site electron hopping outweighs spin-lattice coupling, since the latter would give a negative contribution to J_{bq} [11, 12]. Crucially, we quantify the magnetic interactions that stabilize the noncoplanar state, in contrast to other proposed 3- \mathbf{q} structures in NiS_2 [63–65], MnTe_2 [66], and UO_2 [67–70], where the relevant interactions are not yet well understood. Our work provides several guiding principles to facilitate the identification of multi- \mathbf{q} spin textures. First, the near-degeneracy of 1- \mathbf{q} and multi- \mathbf{q} structures on the FCC lattice makes double perovskites enticing systems. In candidate materials, the crystal symmetry should be higher than a 1- \mathbf{q} model would imply. Second, magnets that are not deep inside the Mott-insulating regime are expected to have larger J_{bq} and, consequently, more robust 3- \mathbf{q} orderings. This criterion hints that cubic Ba_2YO_6 [71, 72] may also host a 3- \mathbf{q} state, due to its extended $5d$ orbitals, potentially offering a route to investigate the effect of increased electron hopping. For small J_{bq} , we anticipate a thermally-induced transition from 3- \mathbf{q} to 1- \mathbf{q} ordering, since thermal fluctuations fa-

vor collinear states. Third, quartic single-ion anisotropy may play a role in FCC magnets with $S > 3/2$; in particular, easy- $\langle 111 \rangle$ axis anisotropy should favor $3\text{-}\mathbf{q}$ ordering. Finally, our key methodological insight is that refining the magnetic structure and interactions simultaneously enables $1\text{-}\mathbf{q}$ and multi- \mathbf{q} structures to be distinguished on the FCC lattice, even when single-crystal samples are not available.

This work was supported by the U.S. Department of Energy, Office of Science, Basic Energy Sciences, Materials Sciences and Engineering Division. This research used resources at the Spallation Neutron Source, a DOE Office of Science User Facility operated by the Oak Ridge National Laboratory.

* paddisonja@ornl.gov

† christiansad@ornl.gov

- [1] Y. Tokura, N. Kanazawa, *Chem. Rev.* **121**, 2857 (2021).
- [2] R. Shindou, N. Nagaosa, *Phys. Rev. Lett.* **87**, 116801 (2001).
- [3] W. Feng, *et al.*, *Nature Communications* **11**, 118 (2020).
- [4] C. Sürgers, G. Fischer, P. Winkel, H. v. Löhneysen, *Nature Communications* **5**, 3400 (2014).
- [5] J. Zhou, *et al.*, *Phys. Rev. Lett.* **116**, 256601 (2016).
- [6] T. Kurumaji, *et al.*, *Science* **365**, 914 (2019).
- [7] M. Hirschberger, *et al.*, *Nat. Commun.* **10**, 5831 (2019).
- [8] M. Hirschberger, *et al.*, *Phys. Rev. Lett.* **125**, 076602 (2020).
- [9] S. Gao, *et al.*, *Nature* **586**, 37 (2020).
- [10] O. Gomonay, V. Baltz, A. Brataas, Y. Tserkovnyak, *Nat. Phys.* **14**, 213 (2018).
- [11] K. Penc, N. Shannon, H. Shiba, *Phys. Rev. Lett.* **93**, 197203 (2004).
- [12] F. Wang, A. Vishwanath, *Phys. Rev. Lett.* **100**, 077201 (2008).
- [13] M. V. Gvozdkova, M. E. Zhitomirsky, *J. Exp. Theor. Phys. Lett.* **81**, 236 (2005).
- [14] R. Schick, T. Ziman, M. E. Zhitomirsky, *Phys. Rev. B* **102**, 220405 (2020).
- [15] R. R. P. Singh, W. Zheng, J. Oitmaa, O. P. Sushkov, C. J. Hamer, *Phys. Rev. Lett.* **91**, 017201 (2003).
- [16] P. A. McClarty, P. Stasiak, M. J. P. Gingras, *Phys. Rev. B* **89**, 024425 (2014).
- [17] P. A. Maksimov, Z. Zhu, S. R. White, A. L. Chernyshev, *Phys. Rev. X* **9**, 021017 (2019).
- [18] J. Jensen, P. Bak, *Phys. Rev. B* **23**, 6180 (1981).
- [19] B. Hålg, A. Furrer, *Phys. Rev. B* **34**, 6258 (1986).
- [20] K. Hirai, T. Jo, *J. Phys. Soc. Jpn* **54**, 3567 (1985).
- [21] S. Kawarazaki, *et al.*, *Phys. Rev. Lett.* **61**, 471 (1988).
- [22] S. Kawarazaki, Y. Sasaki, K. Yasuda, T. Mizusaki, A. Hirai, *J. Phys.: Condens. Matter* **2**, 5747 (1990).
- [23] M. W. Long, O. Moze, *J. Phys.: Condens. Matter* **2**, 6013 (1990).
- [24] R. S. Fishman, *et al.*, *Phys. Rev. B* **61**, 12159 (2000).
- [25] J.-P. Hanke, F. Freimuth, S. Blügel, Y. Mokrousov, *Sci. Rep.* **7**, 41078 (2017).
- [26] N. D. Khanh, *et al.*, *Nat. Nanotechnol.* **15**, 444 (2020).
- [27] D. F. Agterberg, S. Yunoki, *Phys. Rev. B* **62**, 13816 (2000).
- [28] S. Hayami, Y. Motome, *Phys. Rev. B* **90**, 060402 (2014).
- [29] T. Jo, *J. Phys. F: Met. Phys.* **13**, L211 (1983).
- [30] Y. Matsuura, T. Jo, *J. Phys. Soc. Jpn* **78**, 124709 (2009).
- [31] S. Hayami, Y. Motome, *Phys. Rev. B* **103**, 054422 (2021).
- [32] S. Hayami, Y. Motome, *J. Phys.: Condens. Matter* **33**, 443001 (2021).
- [33] J. Kouvel, J. Kasper, *J. Phys. Chem. Solids* **24**, 529 (1963).
- [34] P. Battle, C. Jones, *J. Solid State Chem.* **78**, 108 (1989).
- [35] J. P. Carlo, *et al.*, *Phys. Rev. B* **88**, 024418 (2013).
- [36] T. Aharen, *et al.*, *Phys. Rev. B* **80**, 134423 (2009).
- [37] G. J. Nilsen, C. M. Thompson, G. Ehlers, C. A. Marjerrison, J. E. Greedan, *Phys. Rev. B* **91**, 054415 (2015).
- [38] A. M. Cook, S. Matern, C. Hickey, A. A. Aczel, A. Paramakanti, *Phys. Rev. B* **92**, 020417 (2015).
- [39] P. Balla, Y. Iqbal, K. Penc, *Phys. Rev. Research* **2**, 043278 (2020).
- [40] S.-S. Diop, G. Jackeli, L. Savary, *Phys. Rev. B* **105**, 144431 (2022).
- [41] R. Schick, *et al.*, *arXiv* p. 2206.12102 (2022).
- [42] S. Gangopadhyay, W. E. Pickett, *Phys. Rev. B* **93**, 155126 (2016).
- [43] A. Paramakanti, *et al.*, *Phys. Rev. B* **97**, 235119 (2018).
- [44] J.-W. G. Bos, J. P. Attfield, *Phys. Rev. B* **70**, 174434 (2004).
- [45] A. E. Taylor, *et al.*, *Phys. Rev. B* **93**, 220408 (2016).
- [46] A. E. Taylor, *et al.*, *Phys. Rev. B* **98**, 214422 (2018).
- [47] S. Gao, *et al.*, *Phys. Rev. B* **101**, 220412 (2020).
- [48] A. Paramakanti, D. D. Maharaj, B. D. Gaulin, *Phys. Rev. B* **101**, 054439 (2020).
- [49] D. D. Maharaj, *et al.*, *Phys. Rev. Lett.* **124**, 087206 (2020).
- [50] N. Iwahara, V. Vieru, L. F. Chibotaru, *Phys. Rev. B* **98**, 075138 (2018).
- [51] Y.-W. Fang, R. Yang, H. Chen, *J. Phys.: Condens. Matter* **31**, 445803 (2019).
- [52] See supplemental material for synthesis details, experimental and computational methods, and two supplemental figures.
- [53] G. E. Granroth, *et al.*, *J. Phys.: Conf. Ser.* **251**, 012058 (2010).
- [54] A. P. Cracknell, B. L. Davies, S. C. Miller, W. F. Love, *Kronecker Product Tables. General Introduction and Tables of Irreducible Representations of Space Groups*, vol. 1 (Plenum, 1979).
- [55] A. Wills, *J. Phys. IV France* **11**, 133 (2001).
- [56] P. J. Brown, *International Tables for Crystallography* (Kluwer Academic Publishers, Dordrecht, 2004), vol. C, chap. Magnetic Form Factors, pp. 454–460.
- [57] J. A. M. Paddison, *et al.*, *npj Quantum Materials* **6**, 99 (2021).
- [58] J.-P. Ader, *Phys. Rev. B* **65**, 014411 (2001).
- [59] S. Toth, B. Lake, *J. Phys.: Condens. Matter* **27**, 166002 (2015).
- [60] D. Dahlbom, *et al.*, Renormalized classical theory of quantum magnets. In preparation.
- [61] A. A. Aczel, *et al.*, *Phys. Rev. B* **93**, 214426 (2016).
- [62] Z. Wang, P. Zhang, J. Shi, *Phys. Rev. B* **76**, 094406 (2007).
- [63] K. Kikuchi, T. Miyadai, T. Fukui, H. Itô, K. Takizawa, *J. Phys. Soc. Jpn* **44**, 410 (1978).
- [64] K. Yosida, S. Inagaki, *J. Phys. Soc. Jpn* **50**, 3268 (1981).
- [65] T. Higo, S. Nakatsuji, *J. Phys. Soc. Jpn* **84**, 053702 (2015).
- [66] P. Burlet, *et al.*, *Phys. Rev. B* **56**, 14013 (1997).
- [67] B. C. Frazer, G. Shirane, D. E. Cox, C. E. Olsen, *Phys. Rev.* **140**, A1448 (1965).
- [68] J. Faber, G. H. Lander, *Phys. Rev. B* **14**, 1151 (1976).
- [69] R. Caciuffo, *et al.*, *Phys. Rev. B* **59**, 13892 (1999).
- [70] S. L. Dudarev, *et al.*, *Phys. Rev. Materials* **3**, 083802 (2019).
- [71] E. Kermarrec, *et al.*, *Phys. Rev. B* **91**, 075133 (2015).
- [72] D. D. Maharaj, *et al.*, *Phys. Rev. B* **98**, 104434 (2018).